Reaction Chemistry & Engineering

ROYAL SOCIETY OF CHEMISTRY

REVIEW

View Article Online
View Journal | View Issue

Cite this: *React. Chem. Eng.*, 2020, **5**, 2204

Cyclic redox scheme towards shale gas reforming: a review and perspectives

Lang Qin, †[a] Zhuo Cheng, †[a] Deven Baser, †[a] Tyler Goldenbaum, [a] Jonathan A. Fan[b] and Liang-Shih Fan *[a]

Received 20th July 2020,
Accepted 5th October 2020

DOI: 10.1039/d0re00301h

rsc.li/reaction-engineering

Alkanes are potential precursors to many value-added chemicals such as olefins and other petrochemicals. However, the conversion of light alkanes can be challenging due to their strong C–H bonds. Chemical looping technology based on cyclic redox schemes is an attractive platform that utilizes metal oxides as oxygen carriers for clean and effective fuel processing. Chemical looping systems can potentially be operated over a wide range of reaction conditions with a lower capital and operating cost under a reduced energy and environmental penalty. The reactivity and long-term performance of the oxygen carriers are key for the successful deployment of the chemical looping technology. This work reviews the recent advances in chemical looping alkane utilization including chemical looping partial oxidation (CLPO) of methane, chemical looping oxidative coupling of methane (CLOCM) and oxidative dehydrogenation (CLODH) of ethane, propane and butane. In particular, material design, mechanistic insights of the reactions, and associated reactor configurations for the reactions are discussed. The perspective viewpoints are also given on the viability of the cyclic redox schemes for shale gas dehydrogenation/reforming applications.

1. Introduction

The advanced technological developments in horizontal drilling and hydraulic fracturing have contributed to a growing production capacity of shale gas in the U.S.[1–3] The U. S. Energy Information Administration estimates that the annual domestic shale gas production will increase by 104% from 9.7 trillion cubic feet in 2012 to 19.8 trillion cubic feet in 2040.[4] As the main components in shale gas, light alkanes (C = 1–4) are potential precursors towards value-added chemical production due to their lack of low-lying vacant orbitals or lone pair electrons.[5] Light alkanes are composed of C–C and C–H bonds which consist of strongly localized electron pairs; they are relatively inert, exhibiting little or no reactivity at conditions typical for activating functional group reactions in other organic compounds. One possibility to

[a] *William G. Lowrie Department of Chemical and Biomolecular Engineering, The Ohio State University, 151 W. Woodruff Ave, Columbus, OH 43210, USA. E-mail: fan.1@osu.edu*
[b] *Department of Electrical Engineering, Ginzton Laboratory, Spilker Engineering and Applied Sciences, Stanford University, 348 Via Pueblo Mall, Stanford, CA 94305, USA*
† These authors contributed equally.

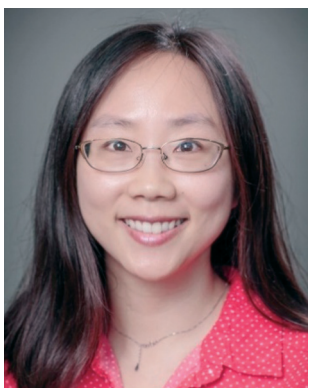

Lang Qin

Dr. Lang Qin is a research associate at the Department of Chemical and Biomolecular Engineering, The Ohio State University. She received her BS degree in chemistry from Peking University (China) and her PhD degree in physics from Salford University (UK). Her current research focuses on the design and mechanism study of microscale and nanoscale materials in chemical looping energy conversion and utilization.

Zhuo Cheng

Dr. Zhuo Cheng is a research associate and engineer in the Department of Chemical and Biomolecular Engineering at The Ohio State University. He obtained his PhD degree in energy, environmental and chemical engineering from Washington University in 2014. His research interests encompass chemical engineering, catalysis science and computational chemistry with emphasis on energy-related applications.

utilize these light alkanes is by acquiring the stored energy in the C–C and C–H bonds as heat energy through full combustion. Another possibility of utilization is to obtain value-added chemicals with permissible in-between oxidation states of carbon from light alkane reforming.[6] The combustion reaction has limited applications for chemical production and is associated with massive CO_2 production; hence, it is of great importance to develop economic and environmentally friendly processes for light alkane reforming to the desired target compounds that contain at least one carbon atom that can be assigned an oxidation number between −4 and +4.[7–10] In the past few decades, the topic of alkane reforming has been sought after by many researchers in a number of research domains including catalysis, photocatalysis and electrocatalysis. Commercially viable processes of alkane reforming have also been developed in industry. In the state-of-the-art commercial processes, steam reforming, steam cracking and fluid catalytic cracking are the dominant technologies used for industrial production of synthesis gas (syngas), ethylene or propene.[11] However, the growth in demand for next-generation materials and processes with higher performance and lower capital costs may outpace the established systems in the near future. In this article, we will focus on the emerging technology[12] that integrates the recent advances in materials design and reaction engineering in a cyclic redox scheme.

The concept of redox reactions has been adopted in a number of fields such as batteries,[13] photocatalysis,[14–16] electrochemistry and chemical looping[12] in which electrons or ions are subjected to multiple cycles of reactions in a chemistry process of energy generation or high value chemical production. Metal oxide materials are widely used in these processes, generating pairs of electrons and holes or ions and vacancies. Among these processes, chemical looping is one of the most attractive and efficient platforms that is capable of large-scale production of syngas and other value-added chemicals.[12,17–20] The chemical looping process typically involves two reactors, a reducer and a combustor. As shown in Fig. 1, in the reducer, metal oxide oxygen carriers react with alkanes to produce syngas or value-added chemicals while the oxygen carriers are reduced to a lower oxidation state. In the combustor, the reduced oxygen carriers are regenerated by air and the fully oxidized oxygen carriers are recycled in the reducer.[12] The oxygen carrier supplies lattice oxygen to the alkanes, thus avoiding the direct contact of air with the fuel and eliminating the need for an air separation unit (ASU) and also the hazards associated with flammable hydrocarbon/O_2 mixtures. More recently, interest in chemical looping technology also stems from the easiness in its CO_2 emission control in comparison to other CO_2 emission control methodologies.[12] The intrinsic nature of chemical looping lies in the redox reactions involving feedstock molecule adsorption and dissociation on metal-oxide-based oxygen carrier surfaces, lattice oxygen ion diffusion and oxygen vacancy creation and annihilation.[12,21,22] The state-of-the-art chemical looping technology has achieved a continuous operation over thousands of cycles.[23] Consequently, chemical looping is an ideal platform for commercialization for alkane reforming. This article provides a review and perspectives on the recent chemical looping technology applications for light alkane reforming involving in particular the three most intensively investigated chemical looping reaction routes illustrated in Fig. 1. These routes include those for chemical looping

Deven Baser

Deven Baser is a recent graduate (2020) from The Ohio State University with a doctorate degree in chemical engineering. He was a graduate research associate in Dr. L.-S. Fan's research group with his research focused on material and process development of various chemical looping systems in the energy and environmental sectors. He received his BS degree in 2015 in chemical engineering from the Institute of Chemical Technology, India.

Liang-Shih Fan

Liang-Shih Fan is distinguished university professor and C. John Easton professor in engineering at The Ohio State University. His research fields are in particle technology and multiphase reaction engineering. He is an inventor of eight clean fossil energy conversion processes for CO_2, SO_2, and NO_x emission control and electricity, syngas, hydrogen, chemicals or liquid fuel production and the electrical capacitance volume tomography for three-dimensional multiphase flow imaging. Fan is the editor-in-chief of Powder Technology and a member of the U. S. National Academy of Engineering, academician of the Academia Sinica, and a foreign member of the Chinese Academy of Engineering, the Australia Academy of Technology and Engineering, the Indian National Academy of Engineering, and the Mexican Academy of Sciences.

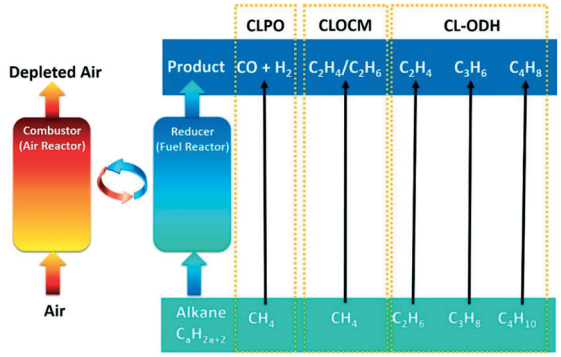

Fig. 1 Overall reactions for the cyclic redox dehydrogenation systems.

partial oxidation (CLPO) of methane, chemical looping oxidative coupling of methane (CLOCM) and chemical looping oxidative dehydrogenation (CLODH) of ethane, propane and butane. The insights into the components of the active sites for C–H activation and dehydrogenation will provide a foundation for rational design of new and efficient chemical looping systems for next-generation shale gas utilization.

2. Chemical looping partial oxidation (CLPO)

Methane is a key component in shale gas and can be converted to syngas through partial oxidation. The conventional methane-to-syngas generation is achieved using catalytic processes such as steam methane reforming or dry (CO_2) reforming which are highly endothermic and operated at a high temperature and high pressure to attain a high conversion rate and to minimize the thermodynamic driving force for carbon deposition. Autothermal reforming (ATR) is an alternative approach with exothermic oxidation of methane reacting with a mixture of oxygen, steam and/or CO_2; nevertheless, a high temperature above 900 °C is required. To reduce these operating temperatures while counteracting carbon deposition, noble metals such as Pt, Pd and Au in metal-based catalysts are generally required. However, the use of noble metals adds to the process cost.[24] On the other hand, methane partial oxidation is an energy-efficient approach and the syngas products have a H_2/CO ratio of 2 which is ideal for gas-to-liquid (GTL) technology. Methane reforming using the chemical looping partial oxidation (CLPO) technology represents the state-of-the-art approach for methane partial oxidation. The approach poses attractiveness from the aspects of process exergy efficiency and economics relative to that of the traditional processes. It is capable of directly producing high-quality syngas with minimal energy penalty and does not require an ASU, water–gas shift reactor, or CO_2 separation unit. A viable CLPO process comprising redox cycles[25] of metal oxide oxygen carriers in two interconnected reactors, *i.e.*, reducer and combustor, is illustrated in Fig. 1. In a CLPO process, lattice oxygen O_O^X in a metal oxide oxygen carrier reacts with methane with formation of oxygen vacancy V_O and syngas products, in reaction (1):

$$CH_4 + O_O^X \rightarrow V_O + 2e + CO + 2H_2 \quad (1)$$

The oxygen carrier with oxygen vacancy V_O is then regenerated by air:

$$\frac{1}{2}O_2 + V_O + 2e \rightarrow O_O^X \quad (2)$$

The majority of the oxygen carrier design is based on microparticles of transition metal oxides[12] due to their lower cost and ease of manufacture, whilst pioneer work in nanoparticles as oxygen carriers are emerging in recent research.[23] Nanoparticle oxygen carriers have larger surface areas and active sites with size-effect enhanced reactivity promotion compared with microparticles, yet they are universally associated with higher production cost and difficulty in large-scale production and may also suffer from surface contamination and significant surface area shrinkage under the harsh chemical looping operational conditions. In the following section we discuss the most recent development in microscale and nanoscale oxygen carriers, respectively.

2.1 Microparticles as oxygen carriers

The main focus of the state-of-the-art CLPO lies in the oxygen carrier design and improvement with relatively limited focus on the reactor design.[26,27] Numerous oxygen carriers have been investigated as candidates for CLPO applications, including the transition metal oxides of manganese, cobalt, nickel, copper, rare earth metals or a combination, which has been summarized in Table 1.[23,28–31] Among all the oxygen carriers, iron oxide oxygen carrier is a cost-effective option with high oxygen carrying capacity and moderate reactivity. The recent process evolution in CLPO of methane with iron-based microparticle oxygen carriers reveals a maximum syngas selectivity of 90% at 1000 °C.[32] However, it remains challenging to concurrently achieve high syngas selectivity and methane conversion at the substantially lower temperatures necessary to develop cost- and energy-efficient processes.[33] Consequently, catalytic dopant-modified Fe_2O_3 microparticle oxygen carriers have been investigated to improve their moderate reactivity. It was found that 1% isovalent lanthanum dopant in Fe_2O_3 can significantly enhance redox reactivity while maintaining or improving the recyclability of iron-based oxygen carriers, as shown in Fig. 2(a)–(c). The reactivity of La-doped oxygen carriers is 178% higher than that of undoped iron oxide oxygen carriers in CLPO of methane (Fig. 2(e)). The mechanism for La dopant-based reactivity enhancement stems from the ability of La dopants to lower the barriers of the C–H bond activation during metal oxide redox reactions (Fig. 2(d)). Nevertheless, oxygen vacancy formation is believed to further promote ionic conductivity in iron-based oxygen carriers, which can be achieved in aliovalent dopants. 1% Cu dopant

Table 1 Summary of the performance of different OCs in the CLPO process[23] (reproduced with permission from the American Chemical Society)

Oxygen carrier	CH_4 concentration (%)	GHSV (mL g^{-1} h^{-1})	Reaction temperature (°C)	CH_4 conversion (%)	H_2 selectivity (%)	CO selectivity (%)
$LaFeO_3$	11	6900	900	63		99
$LaFeO_3$	11	6900	850	32		100
$LaFeO_3$	11	6900	800	6		97
3DOM $LaFeO_3$	40	1200	850	39	84	100
$LaFeO_3/Al_2O_3$–kaolin	11	7800	900	25		70
$La_{0.8}Sr_{0.2}FeO_3$	11	13 800	900	70	>95	>95
$La_{0.7}Sr_{0.3}FeO_3$	40	1200	850	70	82	95
$La_{0.5}Sr0.5FeO_3$	40	1200	850	67	75	85
$La_{0.1}Sr_{0.9}FeO_3$	40	1200	850	57	76	87
$La_{0.9}Sr_{0.1}FeO_3$	40	1200	800	82	98	97
$La_{0.7}Sr_{0.3}FeO_3$	40	1200	800	39	78	98
$La_{0.5}Sr_{0.5}FeO_3$	40	1200	800	52	83	100
$La_{0.1}Sr0._9FeO_3$	40	1200	800	37	60	100
$LaMnO_3$	11	13 800	900		66	53
$La_{0.8}Sr_{0.2}MnO$	11	13 800	900		78	58
Fe_2O_3@$La_{0.8}Sr_{0.2}FeO_{3-\delta}$	10	600 000	900		80	87
Fe_2O_3@$La_{0.8}Sr_{0.2}FeO_{3-\delta}$	10		900		84	82
Fe_2O_3@$La_{0.7}Sr_{0.3}FeO_{3-\delta}$	10		900		84	86
Fe_2O_3@$La_{0.5}Sr_{0.5}FeO_{3-\delta}$	10		900		70	80
Fe_2O_3@$LaFeO_3$	10		900		64	85
Fe_2O_3@$SrFeO_3$	10		900		40	64
$La_{1.6}Sr_{0.4}FeCoO_6$	37	3600	800	65	77	100
Mg–$La_{1.6}Sr_{0.4}FeCoO_6$	37	3600	800	75	97	100
Li–$La_{1.6}Sr_{0.4}FeCoO_6$	37	3600	900	40	88	100
$La_{1.6}Sr_{0.4}FeCoO_6$	37	3600	900	86		100
Mg–$La_{1.6}Sr_{0.4}FeCoO_6$	37	3600	900	98		100
Rh/$La_{0.75}Sr_{0.25}(Fe_{0.8}Co_{0.2})_{0.75}Ga_{0.25}O_{3-\delta}$	10		600	83		97
$CaMn_{0.8}Ni_{0.2}O_3$	10	60 000	900			63
$CaMn_{0.8}Fe_{0.2}O_3$	10	60 000	900			68
$BaMn_{0.75}Fe_{0.25}O_3$	10	60 000	900			95
$BaMn_{0.75}Ni_{0.25}O_3$	10	60 000	900			94
$CaMnO_3$	37	120 000	500			2
Rh/$CaMnO_3$	37	120 000	500		100	88
$CaMnO_3$	37	120 000	600			5
Rh/$CaMnO_3$	37	120 000	600		97	86
$CaMnO_3$	37	120 000	700			12
Rh/$CaMnO_3$	37	120 000	700			57
$CaMnO_3$	37	120 000	800			27
Rh/$CaMnO_3$	37	120 000	800			48
Rh/$CaMnO_3$	37	120 000	900			45
$CaMnO_3$	37	120 000	900			40
$LaCeO_{3.5}$	37	120 000	600			4
Rh/$LaCeO_{3.5}$	37	120 000	600			98
$LaCeO_{3.5}$	37	120 000	700			52
Rh/$LaCeO_{3.5}$	37	120 000	700		100	99
Rh–$CaMnO_3$	25	13 000	600	20	66	81
Rh–$CaMn_{0.95}Fe_{0.05}O_3$	25	13 000	600	10	2	
Rh–$CaMn_{0.75}Fe_{0.25}O_3$	25	13 000	600	7	3	2
Rh–$Ca_{0.95}Sr_{0.05}MnO_3$	25	13 000	600	8	49	41
Rh–$Ca_{0.75}Sr_{0.25}MnO_3$	25	13 000	600	12	52	44
$BaFe_3Al_9O_{19}$	5	4500	900	86		83
CeO_2/Al_2O_3	100		900	85	65	65
CeO_2/MgO	100		900	65	42	40
CeO_2/TiO_2	100		900	62	48	52
CeO_2/γ-Al_2O_3			925	76	95	97
Fe_2O_3	100	333	900	16	30	33
CeO_2	100	333	900	28	99	97
$Ce_{0.2}Fe_{0.8}O_2$	100	333	900	86	62	68
$Ce_{0.4}Fe_{0.6}O_2$	100	333	900	95	90	98
$Ce_{0.8}Fe_{0.2}O_2$	100	333	900	46	100	98
$Ce_{0.6}Fe_{0.4}O_2$	100	333	900	94	95	90
$ZrO_2/Ce_{0.7}Fe_{0.3}O_2$	100	333	800	65	84	84
$Ce_{0.7}Zr_{0.3}O_2$	100	333	850	15	80	79
$Ce_{0.6}Zr_{0.3}Cu_{0.1}$	5		850	75		95
$Ce_{0.7}Zr_{0.3}O_2$	100	333	800	41	80	80

Table 1 *(continued)*

Oxygen carrier	CH_4 concentration (%)	GHSV (mL g^{-1} h^{-1})	Reaction temperature (°C)	CH_4 conversion (%)	H_2 selectivity (%)	CO selectivity (%)
$Zr_{0.7}Fe_{0.3}O_2$	100	333	800	45	81	91
$Ce_{0.5}Ni_{0.5}O_2$	100	333	800	95	43	42
$Ce_{0.7}Ni_{0.3}O_2$	100	333	800	92	56	57
Pr–Ce–Zr			800	55	54	71
Gd–Ce–Zr			800	49	51	47
La–Ce–Zr			800	46	45	44
WO_3	10	18 000	800	11	59	94
WO_3/Al_2O_3	10	18 000	800	21	89	90
$Ni_{0.3}WO_x/Al_2O_3$	10	18 000	800	42	93	93
$Ni_{0.5}WO_x/Al_2O_3$	10	18 000	800	59	94	92
$NiWO_x/Al_2O_3$	10	18 000	800	45	99	95

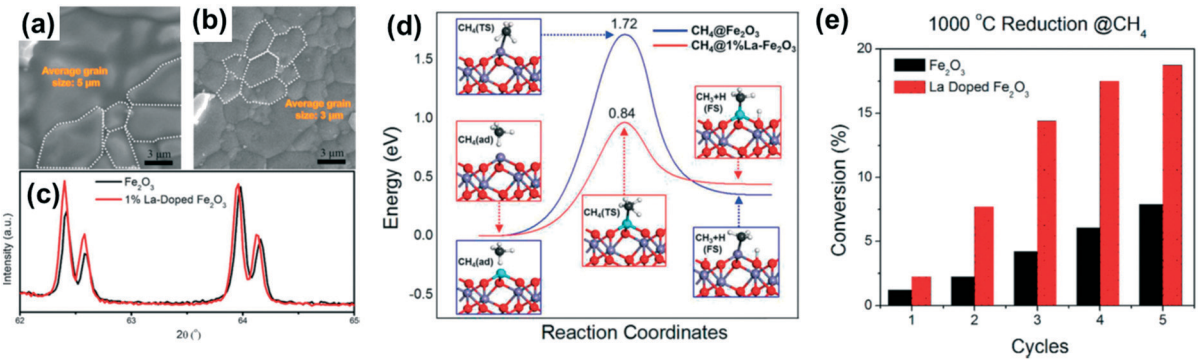

Fig. 2 (a) Undoped Fe_2O_3 and (b) La-doped Fe_2O_3; (c) small-range XRD spectra of La-doped Fe_2O_3 and undoped Fe_2O_3; (d) reaction pathway in CLPO of methane with La-doped Fe_2O_3 oxygen carrier; (e) performance test in undoped and La-doped Fe_2O_3 oxygen carrier[34] (reproduced with permission from the American Chemical Society).

results in the lowest cost increase while improving the reactivity of oxygen carriers significantly to a higher extent than La dopant (Fig. 3).[34] Cu-doped Fe_2O_3 has shown over 470% higher reactivity improvement compared with undoped Fe_2O_3 at 700 °C, allowing for an energy consumption savings of 35% (Fig. 3(a)–(d)). A mechanistic insight in Fig. 3(e) has pointed out that an aliovalent dopant may promote oxygen vacancy formation which enhances oxygen ion transport in iron oxide oxygen carriers.[33]

Consequently, a low concentration (~1%) doping strategy can be powerful with minimal cost increase in the oxygen carrier systems. This strategy is likely to be adopted in many other oxygen carrier designs in the future. Perovskite materials have also been studied and found to have high performance. The significant progress in perovskite microparticle oxygen carriers has been well summarized elsewhere.[23] The future challenges of perovskite materials lie in decreasing the material production cost and increasing oxygen carrying capacity.

2.2 Highly selective nanoparticle oxygen carriers

Mesoporous supports possess large surface areas and high thermal stability[35] with controllable pore structure and pore size distribution. The adjustable structural features in mesoporous supports can facilitate reactant mass transfer and can be tailored to enhance the efficiency of the catalytic processes and reaction kinetics. Considerable interest has been directed to exploring nanoscale redox systems in alkane conversion and utilization supported by mesoporous materials. Liu *et al.*[25] demonstrated that the co-production of CO_2 can be significantly suppressed in methane partial oxidation reactions using iron oxide nanoparticles embedded in a mesoporous silica matrix (SBA-15) with a large surface area and narrow hexagonal nanochannels.[25] They experimentally obtained near 100% CO selectivity in a cyclic redox system at 750–935 °C, which is a significantly lower temperature range than in microparticle oxygen carrier systems (Fig. 4). The enhanced selectivity and reactivity is due to the size effect in nanoparticles of 3–8 nm. Experimental results and density functional theory (DFT) calculations elucidate the origins of the size effect and show that low-coordinated lattice oxygen atoms on the surface of nanoparticles significantly promote Fe–O bond cleavage and CO formation. Chemical looping dehydrogenation with steam is derived from partial oxidation. Instead of using air as an oxidant, this system uses steam to regenerate oxygen carriers. In this scheme, nickel-based oxygen carriers were of high interest due to their ability to enhance the methane reaction rate.[36] NiO was embedded in mesoporous SBA-15 and

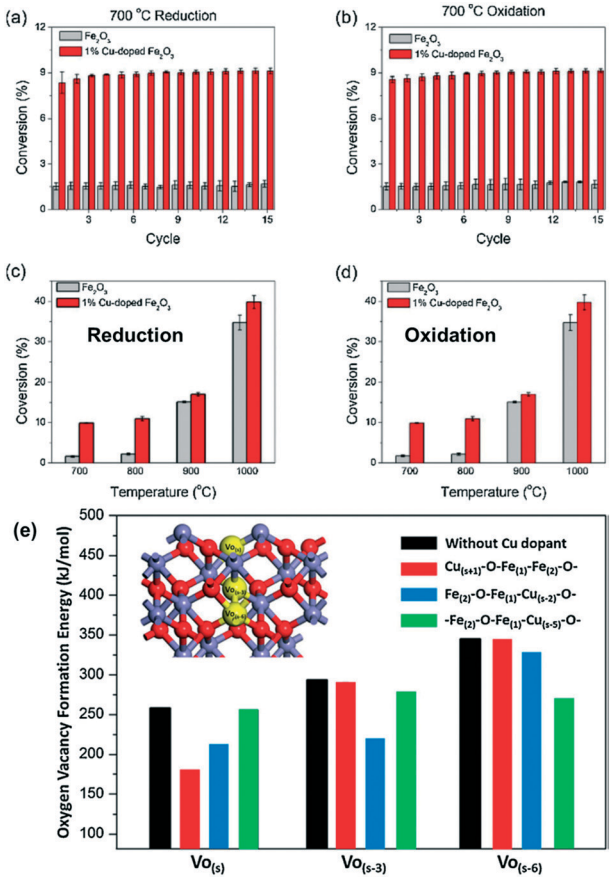

Fig. 3 CLPO of methane to syngas conversion rates in (a) reduction cycles and (b) oxidation cycles. Conversion rates at different temperatures: (c) reduction and (d) oxidation. (e) Cu dopant induced oxygen vacancy formation energy in Cu-doped Fe_2O_3 oxygen carrier[33] (reproduced with permission from Elsevier).

showed a high catalytic activity. However, the Ni active sites quickly deactivated due to carbon deposition.[12] One approach to sustain their activity is to use SBA-16, a mesoporous silica support with a cubic structure and higher mass transfer kinetics.[37] SBA-16 can be modified by incorporating a promoter to aid in improving the mobility of the surface oxygen and hence lowering the carbon deposition on active sites. One promising promoter is CeO_2 for which 15Ni/Ce-SBA-16(40) was shown to promote the dispersion of the NiO particles and prevent the formation of coke.[35] Overall, the methane conversion is increased by 13.7% compared to a traditional chemical looping steam reforming system without a promoter, in addition to an increase in temperature that provides a higher reactivity.[35]

The majority of nanoscale oxygen carriers exhibit much higher reactivity compared with microparticle oxygen carriers. However, they suffer substantially from severe sintering which leads to particle agglomeration and decreased surface areas after redox cycles. The sintering effect can only be mitigated by using nanoscale porous supports such as mesoporous titania, silica and alumina. The potentially high cost of such materials is a future problem to solve.

2.3 Reactor design in the CLPO process

The CLPO of methane process was first developed in the Welty process which consists of two separate fluidized bed reactors.[12] By properly controlling the fuel-to-oxygen carrier ratio, the CO-rich syngas can be generated. Researchers at Chalmers University of Technology in Sweden have investigated the CLPO process in a 300 W_{th} two-compartment fluidized bed reactor system using Ni-based oxygen carriers.[12] In addition, Vienna University of Technology in Austria has

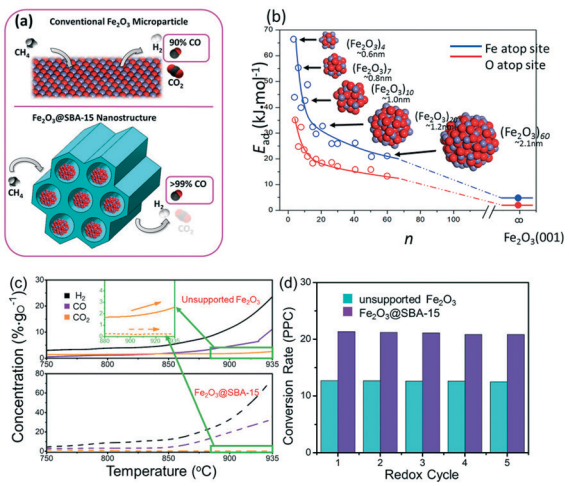

Fig. 4 (a) Illustration of Fe_2O_3@SBA-15, (b) size effect by DFT simulation, (c) TPR in CLPO and (d) redox cycles in CLPO[25] (reproduced with permission from Springer Nature).

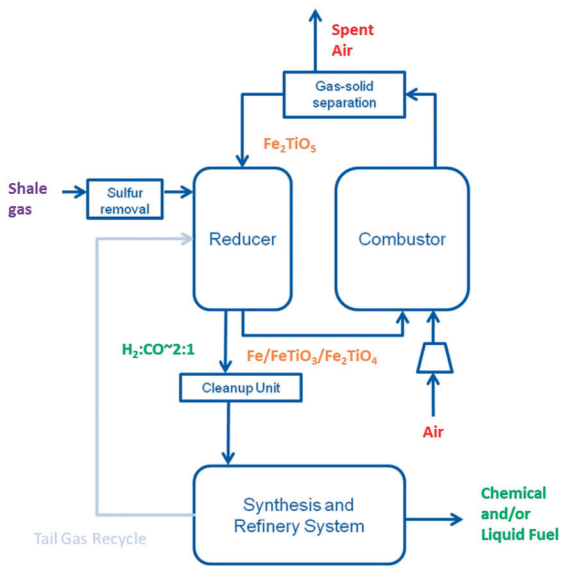

Fig. 5 Chemical looping methane partial oxidation process[38] (reproduced with permission from the Royal Society of Chemistry).

developed a 140 kW_{th} dual circulating fluidized bed reactor system adopting Ni-based oxygen carriers.[12] In order to suppress the carbon deposition promoted by the Ni-based oxygen carriers in CLPO, a significant amount of steam is often introduced, resulting in undesirable $H_2:CO$ ratios.[12] Further, it is challenging to apply a fluidized bed for a reducer operation for the CLPO process due to its inherent back-mixing of the bed. Back-mixing prohibits a high conversion of the oxygen carrier, thereby impeding a high yield of syngas and a high system efficiency required of the CLPO process.

In Fig. 5, a shale gas-to-syngas (STS) process is shown.[38] The STS process consists of a co-current downward flow moving bed reducer combined with iron-based metal oxides. It can efficiently generate a high-purity syngas with a desirable $H_2:CO$ ratio of 2:1 with little carbon deposition. By coupling with the downstream methanol synthesis reactor or the Fischer–Tropsch reactor, the STS process can be applied to efficiently produce chemical and liquid fuels.

3. Chemical looping oxidative coupling of methane (CLOCM)

The previous section describes the conversion of methane into syngas which can be used as an intermediate for the production of value-added chemicals. This section focuses on the recent advances in the direct conversion of methane to value-added products *via* chemical looping. Of the several dehydrogenation schemes for the direct conversion of methane, oxidative coupling of methane (OCM) has been one of the most attractive routes from kinetic and thermodynamic aspects.[12,39] OCM involves the conversion of methane to higher hydrocarbons in the presence of oxygen, as shown in Fig. 1. Based on the source of the oxygen, there can be two modes of operation for OCM, the catalytic mode and the chemical looping mode. The catalytic mode, known as the co-feed mode, uses molecular oxygen (O_2) as the oxygen source which is co-fed with methane to a catalyst bed. The reaction in the bed can be given in reactions (3) and (4) as

$$CH_4 + O_2 \rightarrow C_2H_6/C_2H_4 + H_2O \quad (3)$$

$$CH_4 + O_2 \rightarrow CO/CO_2 + H_2O \quad (4)$$

As indicated earlier, the chemical looping mode or redox mode uses lattice oxygen from oxygen carrier particles as the oxygen source that undergoes reduction reaction in a reducer. The reduced oxygen carrier particles then flow to a combustor, as seen in Fig. 1, for their regeneration using air. Similar to the catalytic system, the reducer of the chemical looping system carries out the partial oxidation reaction of methane as given in reactions (5) and (6), while the regeneration of the reduced metal oxide in the combustor follows reaction (7).

$$CH_4 + MO_2 \rightarrow C_2H_6/C_2H_4 + H_2O + MO \quad (5)$$

$$CH_4 + MO_2 \rightarrow CO/CO_2 + H_2O + MO \quad (6)$$

$$MO + O_2 \rightarrow MO_2 \quad (7)$$

Reactions (3) and (5) are the desired reactions; however, as methane is a fuel it combusts either fully or partially to form CO or CO_2, as seen in reactions (4) and (6). These combustion reactions of forming CO or CO_2 are thermodynamically more favored than the desired OCM products and thus lead to reduced overall yields from typical OCM systems.[40–42] Under these situations for OCM reactions, the CLOCM scheme has several advantages over the catalytic system which are illustrated in the following.

3.1 CLOCM: reaction and process considerations compared with the catalytic process

Both the catalytic system and the chemical looping system were extensively investigated by Keller and Bhasin, which laid the foundation for the subsequent studies.[43] In the catalytic system, the co-fed O_2 provides the necessary oxygen source for facilitating OCM reactions; however it also scavenges the radicals, higher hydrocarbons and other such reactive species from the gas phase.[44] Thus, the overall selectivity and yield that the catalytic system can achieve are reduced. This trade-off limits the amount of oxygen that can be co-fed with CH_4, ultimately limiting the CH_4 conversion from the catalytic system as well.[45] The behavior of the co-fed reactions can also be captured from a thermochemistry study for an ideal catalytic system which calculates the upper bound of C_2 yield at 28%. Here, the upper bound is defined as the limitations caused by the secondary undesired reactions of the C_2 products and the restrictions that are created due to the interdependence of several elementary reactions.[46] These reaction limitations and restrictions due to flammability limits have been mitigated through the use of advanced reactor configurations such as membrane reactors or through the use of chemical looping systems.[47,48] Further, the catalytic system can use air as the oxygen source or pure O_2 through an ASU. With air as the oxygen source, the inert N_2 component helps reduce the overoxidation of higher hydrocarbons, hence improving the selectivity of the OCM.[49–51] However, the N_2 has to be separated from the product stream in order the prevent the accumulation of N_2 during the recycle of CH_4. Further, when pure O_2 is used, the downstream separation is simplified; however, it is at the cost of an additional unit requirement, *i.e.*, ASU. Co-feeding O_2 also requires complete conversion of the O_2 in the OCM reactor to ensure that no O_2 is present in the product stream. These disadvantages can be circumvented through the use of the chemical looping system, which utilizes air as the source of oxygen in the regeneration step in the combustor while no N_2 is present in the metal oxide oxidation step in the reducer.

A different aspect of both OCM systems, *i.e.*, the catalytic and the CLOCM systems, can be further elaborated from the viewpoint of the product distribution. For both the catalytic and the CLOCM systems, there are reactions that take place both in the gas phase and in the solid phase. The first step of the reactions involves the formation of CH_3 radicals and they combine in the gas phase to build the chain of hydrocarbons.[52–54] As the gas phase reactions are independent of the catalyst/catalytic oxygen carrier used, the product slate formed across both OCM systems would appear to be similar.[45] That is, the hydrocarbon products that the OCM synthesizes are typically distributed over several compounds with different carbon numbers. For both the catalytic and the CLOCM systems, it has been observed that the hydrocarbon products for the catalytic OCM spanned from C_2 to C_4, whereas the hydrocarbon products for CLOCM spanned from C_2 to C_7.[45,55] This difference can be accounted for by the undesired reactions that evolved from the gas-phase reaction of the higher hydrocarbons and O_2. Thus, any C_{4+} hydrocarbons in a catalytic OCM system are converted to carbon oxides, rendering a lower selectivity of the OCM process.[56,57] Thus, CLOCM provides an attractive reaction scheme compared to catalytic OCM through providing a larger value addition of methane with the production of a larger product slate.

3.2 Oxygen carrier for CLOCM

Extensive research and development on redox capable metal oxides for CLOCM was conducted earlier at Union Carbide and ARCO.[57–59,84] However, in recent years OCM research has seen a shift from CLOCM to catalytic OCM due to the ease in operation and well=developed mechanistic and material insights. Notably, Siluria Technologies have developed the Gemini process which is deemed as the first commercial OCM process. It has been demonstrated in a catalytic reactor with a production capacity of ~1 ton of ethylene.[60–62,85] The specific catalyst formulation in this process, however, has not been disclosed. This shift from CLOCM to the catalytic OCM has resulted in a slower progress in the development of high-performance catalytic oxygen carriers. For CLOCM, mainly Mn-based and La-based catalytic oxygen carriers have been studied.[63] Some formulations that have been tested are summarized in Table 2.[56–70]

Mn-based catalysts and catalytic oxygen carriers have been extensively studied as seen in Table 1, among which $Mn/NaWO_4/SiO_2$ provides a reasonably high OCM activity[71–73] with C_2 selectivity of 70–80% and CH_4 conversion of 20–30%.[74] Further, the high OCM activity in $Mn/NaWO_4/SiO_2$ is attributed to the synergy among the different phases of oxides supported by SiO_2.[75] These results will help identify the active sites that can be modified to improve the OCM activity. As mentioned in section 2.2, the size of the active metal oxide and the morphology play critical roles in determining the activity of the oxygen carrier/catalyst. The use of nanoparticles has not been investigated for CLOCM, potentially due to hurdles such as oxygen carrier stability issues due to sintering; catalytic OCM has reported several nanoparticle catalysts.[76–78] Further, the effect of microcrystal formation on the catalytic OCM performance has also been studied, which is lacking in the CLOCM domain.[79,80] Assuming a similar trend between the OCM catalyst and the oxygen carrier with respect to morphology changes, the formation of stable nanoparticles/microcrystals will aid in

Table 2 CLOCM activity of various catalytic oxygen carriers

Catalytic oxygen carrier	Temperature (°C)	CH_4 conversion (%)	Selectivity (%)		Ref.
			C_2	C_{2+}	
5% Mn/Al_2O_3	800	11.0	45	—	64
5% Mn/SiO_2	800	13.3	37.5	3.8	64
15% Mn/SiO_2	800	26.0	50.6	8.4	64
5% Bi/SiO_2	800	5.1	53.8	4.4	64
5% Ge/SiO_2	800	1.4	63.1	7.9	64
5% In/SiO_2	800	7.3	46.5	5.7	64
5% Pb/SiO_2	800	2.5	38	7.8	64
5% Sb/SiO_2	800	1.2	59.2	2.7	64
5% Sn/SiO_2	800	3.2	48	3.5	64
15% Mn, 5% $Na_4P_2O_7/SiO_2$	800	30	67		57
$Ag–La_2O_3/SiO_2$[a]	750	45	62	—	65
$Mn/NaWO_4/SiO_2$[a]	775	24	80	—	66
$Mn/NaWO_4/SiO_2$[a]	800	29	74	—	71
$Mn/NaWO_4/$*meso*-SiO_2[a]	775	34	73	—	67
1% CeO_2 La_2O_3/SiO_2[a]	800	10	63	—	68
2% CeO_2 La_2O_3/SiO_2[a]	800	6	74	—	68
$Na–Pr_6O_{11}$	800	21	76		59
Natural manganese mineral	850	27	80	—	69
Mg_6MnO_8	850	71	9	0.4	56
$Li–Mg_6MnO_8$	850	69	16	0.8	56
Doped Mg_6MnO_8	840	37	63		70

[a] Diluted CH_4 stream.

the improvement of CH_4 conversion and C_{2+} selectivity.[81] Similar to a typical OCM catalyst, catalytic oxygen carriers also show a trade-off between hydrocarbon selectivity and CH_4 conversion.[72,82,83] In CLOCM reactions, CH_4 reacts readily with the available lattice oxygen in catalytic oxygen carriers, thus ensuring high CH_4 conversion. However, this results in methane overoxidation to carbon oxides or through sequential reaction of C_{2+} hydrocarbons reacting with the lattice oxygen forming carbon oxides. This results in a gradual reduction in C_{2+} selectivity in CLOCM in the initial stage. As the catalytic oxygen carriers continue to donate lattice oxygen, the reduced availability of their lattice oxygen diminishes the overoxidation reactions of C_{2+} products, thus improving the selectivity of the system.[45,72] However, the reduced availability of lattice oxygen also limits CH_4 oxidation and thus the CH_4 conversion decreases with reaction time. Finally, carbon deposition occurs when all lattice oxygen is unavailable, which is highly undesirable as the catalytic surfaces will be deactivated. Two types of lattice oxygen were reported in the catalytic oxygen carrier, typically distinguished as a weakly bound oxygen species and strongly bound oxygen species. These two types of oxygen species originate from different phases that the catalytic oxygen carrier can exhibit, or could be related to the under-coordinate oxygen species that are present on the surface of the oxidized catalytic oxygen carrier.[86] The weakly bound oxygen reduces the C_{2+} selectivity and thus undesirable. A pretreatment of H_2 reduction of the catalytic oxygen carrier was proven to effectively remove the weakly bound species, which was confirmed by the increased selectivity of C_2.[65,68]

3.3 Mechanistic insights of CLOCM

Mechanism study on CLOCM with Mn-based oxygen carriers has been conducted through the combination of density functional theory calculation and experimental investigation. A comprehensive reaction pathway of methane with Mg_6MnO_8-based catalytic oxygen carriers is illustrated in Fig. 6. CH_4 is initially activated to form CH_3 radical;, weakly bound CH_3 radicals will be desorbed from the surface of the oxygen carrier, allowing it to couple with another CH_3 radical and form C_2 products. On the other hand, strongly bound CH_3 radicals will further dehydrogenate to eventually form CO or CO_2 products. This tuning parameter can be utilized to formulate more selective catalytic oxygen carriers through introducing weak binding oxygen vacancies. As shown in Fig. 6, the Li dopant increases the energy barrier towards CH_3 activation, thus enhancing C_2 selectivity.[54]

3.4 Reactor design in the CLOCM process

Different reactor configurations have been investigated for CLOCM, including fluidized bed, fixed bed and moving bed reactor configurations.[45,48] The fluidized bed reactor, especially circulating fluidized bed reactors as proposed by ACRO, has potential to provide superior heat and mass transfer rates as compared to the other two configurations.[72,84] With the established technology on circulating fluidized beds, the scale-up of such a system would present a lower engineering risk for the CLOCM technology. However, a fluidized bed exhibits CSTR-like well-mixed flow patterns, which increases the probability of undesired secondary reactions of C_{2+} products with a catalytic oxygen carrier, thus reducing the overall yield of OCM taking place in the reactor. On the other hand, PFR-like flow patterns such as those exhibited in a fixed bed or a moving bed reactor are potentially beneficial for increasing the CLOCM yield.[87] A detailed study on the different types of reactors that can be used for OCM have been reported by Cruellas *et al.*, which is a necessary addition to this article.[48] Additionally, an OCM plant requires a product processing island to obtain the final products. The different options include the separation of all the hydrocarbon products into their individual components through the use of cryogenic distillation, as seen in Fig. 7.[70] The other process

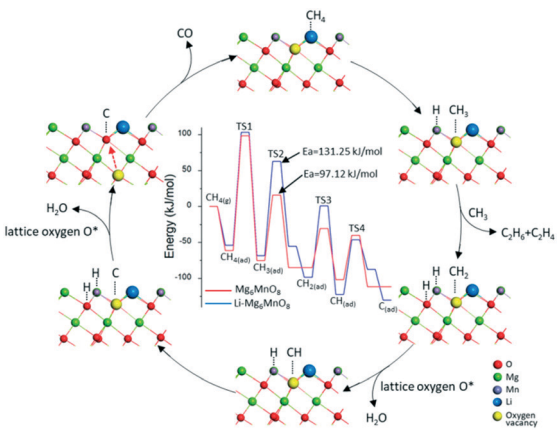

Fig. 6 Proposed reaction mechanism for CLOCM on doped and undoped Mg_6MnO_8 oxygen carriers[54] (reproduced with permission from the American Chemical Society).

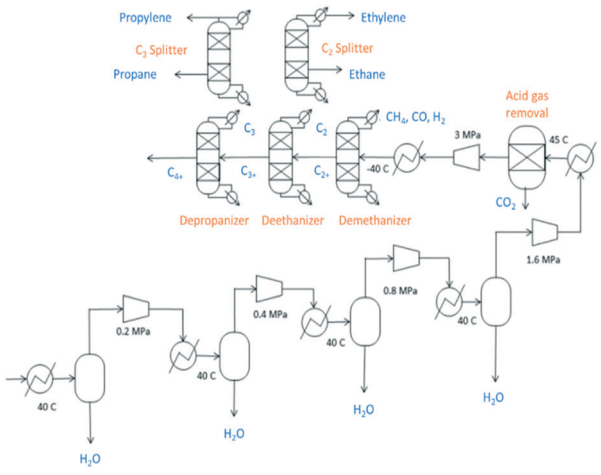

Fig. 7 Cryogenic distillation train for separating the products from OCM systems[70] (reproduced with permission from the American Chemical Society).

configuration generating value-added products involves the use of oligomerization to synthesize gasoline and distillates.[85,86]

The state-of-the-art work generally lacks a techno-economic analysis (TEA) of the CLOCM system. Hence the concept in OCM is adopted to gain insights into the TEA. A TEA analysis of a naphtha steam cracker with respect to catalytic OCM for ethylene production shed light on the drawbacks of the OCM system under several reactor and process configurations. The results of this comparison indicate that ethylene production from OCM is not competitive due to its high capital expense (CAPEX) and electricity demand as compared to naphtha crackers.[87,88] Based on recent estimations, catalytic OCM is expected to be competitive in at least two decades with regard to the forecasted costs of natural gas and ethylene.[87]

For an OCM system, the major cost- and energy-intensive section is the downstream separation units.[12] Both the C_{2+} selectivity and the CH_4 conversion play a crucial role in defining the downstream separation requirements. As mentioned in section 3.1, the elimination of molecular oxygen from the gas phase theoretically improves the C_{2+} selectivity that can be achieved from CLOCM. This would provide additional opportunities for CLOCM to be economically feasible. Further, the TEA of catalytic OCM systems estimate that the ASU accounts for ~8–16% of the bare erected costs, and the majority of the cost is due to the refrigeration units for the cryogenic distillation train and the turbomachines such as compressors and expanders. Further, the ASU required ~12.5–27% of the energy consumed in the catalytic OCM system, adding to the operating cost of producing ethylene.[87,88] These costs can be eliminated in a CLOCM system, thus reducing the dependence of the high CAPEX and operating expense (OPEX) of the OCM system.

4. Chemical looping dehydrogenation of ethane (CLODH-C_2)

Ethylene is conventionally produced through the naphtha or ethane steam cracking process, which is a non-catalytic thermally induced process. Typically, these units are run at 830–840 °C with a steam dilution of 0.4 kg kg^{-1} at the reactor pressure of 1.6–2 atm.[89,90] As this review focuses on the shale gas components, this section focuses on the conversion of ethane to ethylene through the ODH process, and their comparison with steam cracking of ethane. Table 3 depicts a typical product composition from an ethane steam cracking unit. The typical ethane conversion is around 65%, which is close to the thermodynamic limit for the dehydrogenation of ethane as listed in reaction (8).[91]

$$C_2H_6 \rightarrow C_2H_4 + H_2 \quad (8)$$

For such a system the average ethylene selectivity is approximately 80% with an average ethylene yield of 52%. This high activity is accompanied by several process drawbacks that mainly arise due to the endothermic nature of reaction (8).[91,92] On average, the production of one ton of ethylene amounts to 1–1.2 tons of CO_2 due to the heat generated by the furnace. Thus, the ODH system, for both the catalytic and the chemical looping system, provides a pathway to 'combust' the hydrogen from the dehydrogenation product, convert it to H_2O and utilize this exothermic energy to pair with the endothermic heat requirement.

Several catalytic systems and chemical looping systems have been proposed for the ODH of ethane, where the overall reaction is depicted in reaction (9).[71,95–99]

$$C_2H_6 + O_2 \rightarrow C_2H_4 + H_2O \quad (9)$$

CLODH-C_2 has gained a lot of attention due to its unique advantages over the catalytic ODH and the steam cracking of ethane and a detailed review has been published by Li *et al.*[63] Several formulations and morphologies have been tested for CLODH-C_2 which provide a significant improvement over the commercial process, incentivizing a deeper investigation into the reaction mechanism, techno-economic analysis, and eventual commercialization. Compared with ethane steam cracking, the CLODH-C_2 process demonstrates a lower CO_2 emission by 87%.[93] The review by Li *et al.* provides an in-depth perspective of the different types of oxygen carriers that can be used to perform CLODH with different mechanisms which will not be repeated in this article.[63]

Under high-temperature reaction conditions, ethane thermally decomposes into ethylene and hydrogen while the H_2 selectively reacts with the oxygen carrier to produce H_2O. In Mn-based oxygen carriers the selectivity towards CO_x can be limited to 1.9%.[100] The highest performance was reported in a core–shell structure of NaW-promoted Mg_6MnO_8 oxygen carrier, where W was proposed as the active site of the selective oxidation of hydrogen. This composite oxygen carrier exhibits an ethylene yield of 68.2% with a 78% conversion of ethane and an 89.2% selectivity towards ethylene, significantly exceeding the baseline ethane steam cracker unit's performance.[101,102]

Under low-temperature reaction conditions where ethane is unable to be activated thermally, the goal is to activate the C–H bond of ethane to produce ethylene. Several types of

Table 3 Product composition for ethane steam cracker[93,94]

Component	% dry mole
H_2	35.6–37.4
CO–CO_2	0–0.1
CH_4	4.0–5.8
C_2H_2	0.2–0.3
C_2H_4	33.4–34.6
C_2H_6	20.6–25.1
C_3H_6	0.48–0.5
C_3H_8	0.08–0.09
C_4s	0.44–0.54
C_{5+}	0.4–0.5
Others	—

oxygen carriers have been proposed at 500–700 °C, ranging from Mn-based, Fe-based, La-based and V-based mixed metal oxides.[103–105] Under these conditions, Li doped $La_xSr_{2-x}FeO_{4-\delta}$ at 700 °C shows an ethane conversion of 61% and an ethylene selectivity of 90%. The yield of 54.9% is close to that of the ethane steam cracking process at a lower temperature.[103]

5. Chemical looping dehydrogenation of propane and butane (CLODH-C_{3+})

Propane and butane are petroleum gases which are produced during shale gas refining. Compared with C1 and C2, they have a higher energy content. The dehydrogenation of propane and butane to the corresponding alkene products is reversible and highly endothermic, thus higher reaction temperatures are required to achieve high conversions.[106] Further, propane or butane do not effectively convert to their respective olefins as ethane converts to ethylene as seen in Table 3. Both propane and butane tend to crack to C1–C2 products as compared to the dehydrogenated products.[93,94] A temperature of 550–750 °C is typically needed in the dehydrogenation of propane and butane to obtain alkane conversions of over 50% at 1 atm.[107] Chemical looping dehydrogenation of C3 and C4 (CLODH-C_{3+}) is a novel technology for alkene production, which can overcome the thermodynamic equilibrium limitation in non-oxidative dehydrogenation. Similar to chemical looping technologies for methane (C1) and ethane (C2) dehydrogenation, the CLODH-C_{3+} process is also performed in two steps as below:

$$C_{3(4)}H_{8(10)} + MO_x \rightarrow C_{3(4)}H_{6(8)} + MO_{x-1} + H_2O \quad (10)$$

$$MO_{x-1} + 1/2O_2 \rightarrow MO_x \quad (11)$$

In the first step, the oxygen carrier is reduced by propane or butane under the gaseous oxygen-free atmosphere in the fuel reactor; then the reduced oxygen carrier is regenerated by air in the second step to complete a full cycle of the redox reaction. Compared to the conventional ODH process, CLODH-C_{3+} can achieve higher yield because this process reduces deep oxidation by eliminating direct contact between gaseous oxygen and C3/C4 hydrocarbons.[108,109]

5.1 Materials for C3 and C4 dehydrogenation

As an emerging technology, there are only few studies evaluating oxygen carriers for CLODH-C_{3+}. However, the research work on the selection of suitable metal oxide catalysts for ODH of C3 and C4 can be used as the reference for the development of CLODH-C_{3+} oxygen carriers. Since C3 and C4 alkenes are more reactive than their alkane counterparts at high temperature, unwanted side reactions could occur during dehydrogenation, including hydrogenolysis, cracking and isomerization.[110] Hydrogenolysis is a chemical reaction whereby a C–C or C–heteroatom single bond is cleaved by hydrogen. Cracking also results in the C–C bond cleavage to form smaller hydrocarbons, although in this process hydrogen is not required. However, it needs a catalyst to produce a carbocation intermediate.[111,112] Isomerization is a process by which one molecule is transformed into another molecule with a different arrangement and the same atoms. The transformation may occur on a carbocation intermediate or an adsorbed species on the surface of the dehydrogenation catalyst.[113–115] In addition, the high temperature required for the dehydrogenation of C3 and C4 can lead to catalyst deactivation due to coke formation. For example, Pt-based catalysts will deteriorate during the catalytic ODH of propane; thus, it needs to keep reactivating the catalysts to preserve sufficient activity for C–H bond cleavage. The stepwise stoichiometric reactions of oxygen carriers in CLODH-C_{3+} are fundamentally different from conventional ODH, as the former involves ionic diffusion, oxygen vacancy formation and transport both in the bulk and on the surface.[116] The reduced oxygen carriers can be easily regenerated in the oxidizer of chemical looping systems.

Vanadium oxide-based materials have been widely applied for alkane dehydrogenation.[117–122] The active sites on this type of catalysts depend to a large extent on the property of the support and the metal loading.[123] V–O, V–O–V, V═O species or a combination of these species may be present.[124,125] Among these species, V–O is the most active site for propane dehydrogenation.[103,126] Alumina is usually used as the support for vanadium oxide catalysts which can efficiently stabilize V–O-support species. Recently, a propane dehydrogenation experiment was conducted in a bench-scale fluidized reactor under chemical looping conditions using VO_x/CaO–γ-Al_2O_3 as catalytic oxygen carriers. Due to its excellent oxygen carrying capacity, balanced acidity and moderate interaction between active sites and support, 65% propane conversion and 85% propylene selectivity were achieved.[127]

Molybdenum oxides are also commonly used as oxide catalysts in alkane dehydrogenation. The first report of a molybdenum oxide-based catalyst for dehydrogenation was MoO_3/Al_2O_3 used in the dehydrocyclization of *n*-heptane.[128] It was found that Mo–O is highly active for C–H dehydrogenation.[129] The catalytic properties of molybdenum oxide with alumina support for the dehydrogenation of *n*-butane were studied at 560 °C under atmospheric pressure. An *n*-butene selectivity of 80% was obtained with a Mg : Mo molar ratio of 1 : 1. Temperature-programmed reduction tests indicate that Mo was well dispersed on the support. However, if the catalysts were prepared in an acidic medium, the dispersion became worse.[130] Mitchell *et al.* prepared molybdenum hydrotalcite catalysts, which have molybdate intercalated into a hydrotalcite derived from magnesium aluminum hydrotalcite. It was found that the intercalation of molybdate is favored by a low pH (4.5), which is an important factor in affecting the selectivity of the catalysts for propane dehydrogenation.[131]

The dehydrogenation activity of gallium oxide was first reported in the late 1980s.[132] In that report, the conversion of propane to benzenic compounds was studied on various GaHZSM5 catalysts at 530 °C. The results showed that gallium species facilitate propane conversion and enhance the selectivity for aromatics. However, the active sites of gallium-based dehydrogenation catalysts are still unclear. Ga_2O_3 has a monoclinic structure with a high concentration of Lewis acid sites on the surface. It was reported that these sites may serve as the active sites for dehydrogenation.[133] A correlation between the NH_3-TPD results and the initial activity for Ga_2O_3–Al_2O_3 oxides revealed that the population of surface acid sites related to tetrahedral Ga^{3+} cations is a key factor in determining the activity of gallium oxide for C3 or C4 dehydrogenation. Xu *et al.* examined the effect of supports on propane dehydrogenation over gallium oxide catalysts. Their results show that ZrO_2-, TiO_2- and Al_2O_3-supported Ga_2O_3 metal oxides exhibited high activity, but SiO_2- and MgO-supported oxides were not active for propane dehydrogenation. They concluded that the zeolitic support, which includes a low concentration of medium and strong acid sites and a relatively high concentration of weak acid sites, leads to the formation of active species on the surface of Ga_2O_3.[134,135] Recently, Shao *et al.* performed a comprehensive study to examine the support and loading effect on the activity of Ga_2O_3 for propane dehydrogenation. It was found that the support property and the loading amount could significantly influence the textual properties, surface morphologies, acidic properties, surface chemical states, coke formation and dispersion of Ga species. Compared to SBA-15, Al_2O_3- and SiO_2-supported Ga_2O_3, the ZSM-5-supported catalyst exhibit the highest activity as shown in Fig. 8a, since it has the maximum number of well-dispersed gallium species. However, a high Ga loading is unfavorable for the propane dehydrogenation reaction (Fig. 8b) because the Ga species are agglomerated, leading to the deactivation of active sites.[136] An overview of the V-, Mo- and Ga-based metal oxide materials used for the dehydrogenation of C_3H_8 and C_4H_{10} is shown in Table 4. It can be seen that the vanadium oxide-based material has the potential to be an efficient oxygen carrier for CLODH since it achieves not only high conversion but also high selectivity.

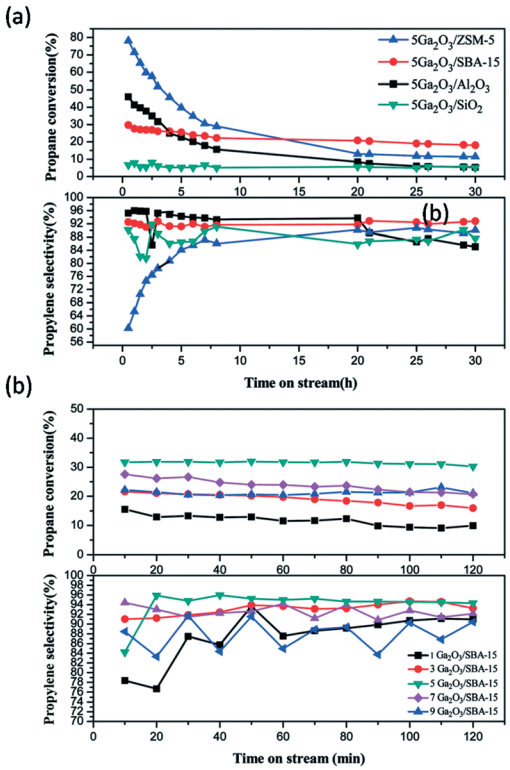

Fig. 8 The effect of (a) the support and (b) Ga_2O_3 content on propane conversion and propylene selectivity (reaction conditions: T = 620 °C; C_3H_8 : Ar (molar ratio) = 1 : 19; WHSV = 0.6 h^{-1}; $m_{cat.}$ = 0.2 g).[136]

Yun *et al.* reported an active propane dehydrogenation catalyst, H-[Fe]ZSM-5, which was prepared by incorporating iron oxides in the framework of ZSM-5 zeolites. H-[Fe]ZSM-5 with a Si/Fe ratio of 26 showed a selectivity of about 85% toward propylene at 773 K. It is generally believed that this dehydrogenation reaction is catalyzed by the extra-framework iron species from iron oxides.[145] Shimada *et al.* investigated the activated carbon-supported iron-based catalyst for the dehydrogenation of isobutane through the redox cycle of Fe_3O_4 and Fe as shown below:[146]

$$C_4H_{10} + Fe_3O_4 \rightarrow i\text{-}C_4H_8 + Fe + H_2O \quad (12)$$

$$Fe + CO_2 \rightarrow Fe_3O_4 + CO \quad (13)$$

The effect of loading level of iron, reaction temperature, time on stream and reaction atmosphere on the isobutane conversion, isobutene yield and isobutene selectivity was investigated. An isobutane conversion of 48%, isobutene yield of 40% and isobutene selectivity of 80% were obtained with 0.3 mmol iron loaded on 1 g of activated carbon at 873 K.

These metal oxides discussed above could be efficient oxygen carriers for the CLODH-C_{3+} process. However, the sintering of oxygen carrier particles might be a substantial problem. In order to improve the anti-sintering ability of the oxygen carriers, their structural stability in redox cycles should be enhanced.

5.2 Process foundation for CLODH-C_{3+}

As mentioned earlier, the dehydrogenation reaction is endothermic and equilibrium limited, requiring temperatures in excess of 600 °C and low-pressure conditions. Based on these requirements, several industrial processes have been developed, two of which currently dominate propylene and butene production: UOP's Oleflex process and Lummus' Catofin process. The UOP Oleflex technology uses a continuous moving bed process with a regenerator as shown in Fig. 9a.[147] The whole system can operate continuously to produce an uninterrupted stream of

Table 4 Summary of the performance of the V-, Mo- and Ga-based metal oxide materials for the dehydrogenation of C_3H_8 and C_4H_{10}

Materials	Reaction temp	Feed	Conversion (%)	Selectivity	Ref.
$VO_x/CaO–\gamma\text{-}Al_2O_3$ (1 : 1)	525–600 °C	C_3H_8	65	85% C_3H_6	127
5% $VO_x/\gamma\text{-}Al_2O_3$	550 °C	C_3H_8	11.7	86% C_3H_6	137
2.2% $VO_x/\gamma\text{-}Al_2O_3$	520 °C	C_4H_{10}	11	55% C_4H_8	138
3.5% $VO_x/\theta\text{-}Al_2O_3$	600 °C	C_4H_{10}	32.9	56% C_4H_8	139
5.2% VO_x/Al_2O_3	580 °C	C_4H_{10}	62	65% C_4H_8	140
17.5% $MoO_3/\gamma\text{-}Al_2O_3$	380 °C	C_3H_8	1.7	83% C_3H_6	141
13.4% MoO_3/Al_2O_3	560 °C	C_4H_{10}	21	50% C_4H_8	142
14.2% MoO_x/SiC	560 °C	C_4H_{10}	22	38% C_4H_8	143
1.7 wt% Ga_2O_3/SiO_2	550 °C	C_3H_8	23	86% C_3H_6	144
5 wt% Ga_2O_3/ZrO_2	600 °C	C_3H_8	39	74% C_3H_6	144
Ga_2O_3/MTS (mesoporous silica)	550 °C	C_4H_{10}	46	58.3% C_4H_8	133

reaction products. In this system, the spherical platinum-based metal particles are applied as catalysts which travel through all of the reactors and then are regenerated. The regenerated catalyst is then transported to the first reactor, completing an entire cycle. The Lummus Catofin technology was developed in the 1940s. It involves a cyclic reactor technology with 5–8 parallel adiabatic fixed-bed reactors going through reaction, reheat and regeneration using a chromia–alumina catalyst developed by Clariant.[148] A schematic of a Catofin dehydrogenation process is shown in Fig. 9b. A comparison of the specifics of these two processes is presented in Table 5.

In UOP's Oleflex process and Lummus' Catofin process, the formation and deposition of coke is unavoidable, leading to a short catalyst life. Therefore, CLODH-C_{3+} technology has the potential to be more efficient in C3 and C4 dehydrogenation applications due to the many reduction and oxidation reactions involved. Recently, Chen *et al.* reported a chemical looping dehydrogenation process for propane dehydrogenation to propylene using a dual-functional Mo–V–O mixed oxide as shown in Fig. 10a.[149] The redox experiments were run *via* dehydrogenation–regeneration cycles without feeding molecular oxygen. Fig. 10b shows the evolution of product compositions over Mo–V–O mixed oxides at 500 °C. Three characteristic regions are identified: overoxidation, oxidative dehydrogenation and nonoxidative dehydrogenation. In the first region, 36% propane conversion and 89% propylene selectivity were achieved, which breaks through the PDH equilibrium yield of 28% *via* at equivalent conditions. During the overall dehydrogenation step, ~80% propylene selectivity and 0.8 mol kg_{cat}^{-1} yield was obtained as shown in Fig. 10c. The propylene yield reported in this work has exceeded that of conventional ODH catalysts due to the involvement and modulation of bulk lattice oxygen *via* Mo doping. This work provides a fundamental insight into the oxygen carrier evolution in the dehydrogenation process and a promising strategy for CLODH-C_{3+} technology. With the development of efficient oxygen carriers, we believe that CLODH-C_{3+} technology has the potential to be commercially deployable in the near future.

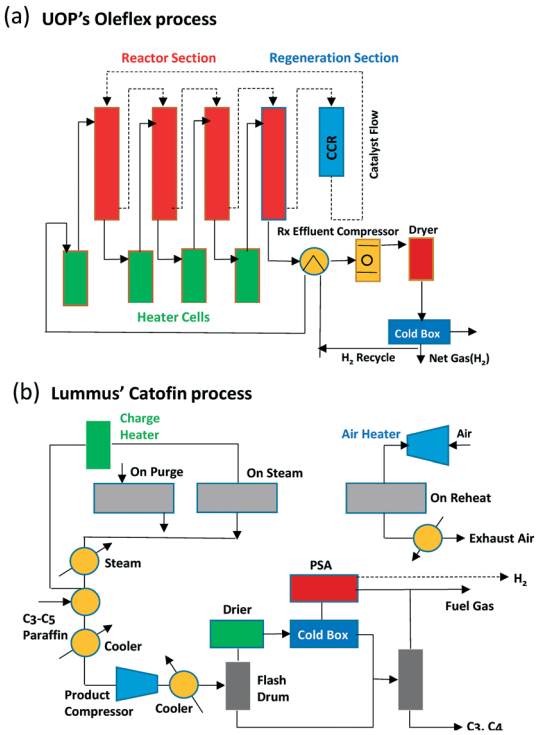

Fig. 9 (a) UOP's Oleflex process flow diagram. (b) Lummus' Catofin process flow diagram.

6. Conclusions and perspectives

Alkanes in shale gas are important feedstocks for value-added chemical conversion. In this article we have reviewed the state-of-the-art chemical looping reforming schemes including the most extensively studied processes CLPO, CLOCM and CLODH. The redox reactions of oxygen carriers in these processes are different from catalytic reforming on conventional catalysts, as the former involves ionic diffusion, oxygen vacancy formation and transport both in the bulk and on the surface of oxygen carriers. The state-of-the-art CLPO of methane process has a major focus on oxygen carrier design and improvement. A design evolution from microparticles to nanoparticles has been readily established with significantly improved performance and properties. In the CLOCM process, mechanistic insights involving the interaction of

Table 5 Comparison of specifics of the Oleflex and Catofin processes

Process	UOP's Oleflex process	Lummus' Catofin process
Reactor system	Continuous moving beds	Fixed beds in parallel
Catalyst	Platinum-based metal catalyst, ~5 year lifetime	Chromia–alumina catalyst ~3 year lifetime
Heating	Using gas flow preheaters	Heating the catalyst during regeneration
Operating conditions	~600 °C, 1–3 bar	~600 °C, 0.5–1 bar
Conversion (%)	35–40	45–50
Selectivity (%)	~90	~90

oxygen vacancies on the surface of the oxygen carrier with CH_x intermediate species are believed to have an impact on the overall yield of C_{2+} products. Additionally, as the oxygen carrier reduction progresses, the overall yield of the C_{2+} products typically decreases, which is a direct result of the reduced availability of oxygen to facilitate CLOCM reactions. This is due to the reduced oxygen diffusion from the bulk to the surface of the oxygen carrier. Thus, the reaction times could be limited to a few seconds of high CLOCM performance, which could be increased as the oxygen diffusion rate can be increased in a controlled fashion through the modification of the oxygen carrier. These considerations could aid in enhancing the viability of the CLOCM process. For CLODH, the state-of-the-art oxygen carrier particles have certain drawbacks due to limited oxygen diffusion from the bulk to the surface. Thus, similar oxygen carrier formulation strategies derived from CLPO and CLOCM can be considered for CLODH. Understanding the mechanisms of the C–C cracking and C–H bond cleavage on the surfaces of oxygen carriers as well as the thermodynamic and kinetic properties of these metal oxide based materials is also essential in successfully engineering cyclic redox reactions towards chemical looping reforming and dehydrogenation of C1–C4 in shale gas.

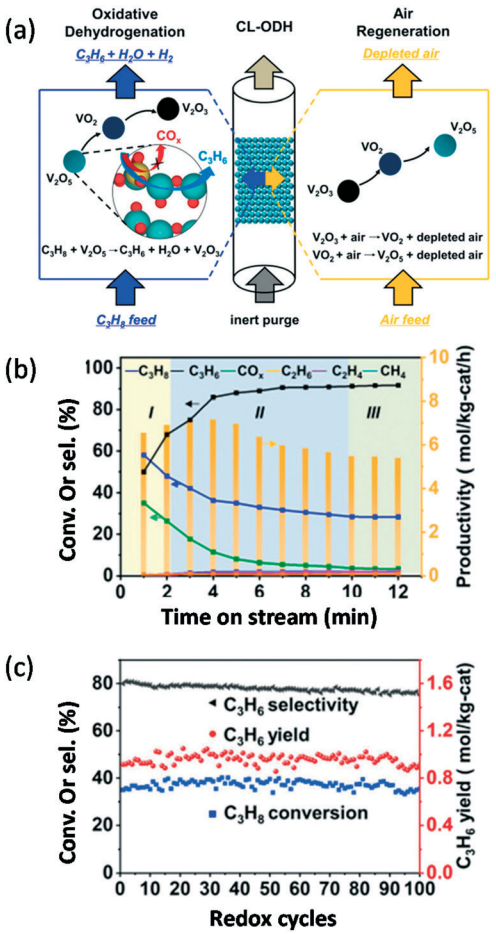

Fig. 10 (a) CLODH scheme. (b) Product profiles over Mo–V–O (V/Mo = 6) with different reaction times. (c) Product profiles over Mo–V–O (V/Mo = 6) during 100 cycles[149] (reproduced with permission from the American Chemical Society).

Author contributions

The manuscript was written through contributions of all authors. All authors have given approval to the final version of the manuscript.

Conflicts of interest

There are no conflicts to declare.

Acknowledgements

The service support provided by the Center for Electron Microscopy and the Analysis and NanoSystem Laboratory at The Ohio State University and the computing support provided by the Ohio Supercomputer Center are gratefully acknowledged.

Notes and references

1 https://www.nytimes.com/2009/10/10/business/energy-environment/10gas.html.
2 https://www.chathamhouse.org/publications/papers/view/185311.
3 U.S. Energy Information Administration, www.eia.gov.
4 https://www.instituteforenergyresearch.org/renewable/wind/eia-forecast-fossil-fuels-remain-dominant-through-2040/.
5 J. A. Lablnger and J. E. Bercaw, *Nature*, 2002, **417**, 507–514.
6 M. B. Smith and J. March, *March's Advanced Organic Chemistry: Reactions, Mechanisms, and Structure*, John Wiley & Sons, Inc, 2007.
7 W. F. Maier, *Angew. Chem., Int. Ed.*, 1999, **38**, 1216–1218.

8 M. Andersen, O. Lytken, J. Engbæk, G. Nielsen, N. Schumacher, M. Johansson and I. Chorkendorff, *Catal. Today*, 2005, **100**, 191–197.
9 J. Greeley and M. Mavrikakis, *Nat. Mater.*, 2004, **3**, 810–815.
10 J. K. Norskov, T. Bligaard, J. Rossmeisi and C. H. Christensen, *Nat. Chem.*, 2009, **1**, 37–46.
11 F. Cavani, N. Ballarini and A. Cericola, *Catal. Today*, 2007, **127**, 113–131.
12 L.-S. Fan, *Chemical looping partial oxidation: gasification, reforming, and chemical syntheses*, Cambridge University Press, 2017.
13 http://www.nexeon.co.uk/about-li-ion-batteries.
14 http://www3.nd.edu/~kamatlab/research_photocatalysis.html.
15 A. Zaleska-Medynska, Metal Oxide-Based Photocatalysis Fundamentals and Prospects for Appl. A vol, in *Metal Oxides Book*, Elsevier, 2018.
16 http://www.protonex.com/technology/solid-oxide-fuel-cell/.
17 L. Zeng, S. Luo, F. Li and L.-S. Fan, *Zhongguo Kexue: Huaxue*, 2012, **42**, 260–281.
18 M. Anheden and G. Svedberg, *Science*, 1998, **39**, 1967–1980.
19 D. Baser, S. Nadgouda, A. Joshi and L.-S. Fan, *Ind. Eng. Chem. Res.*, 2019, **58**(36), 16407–16416.
20 M. V. Kathe, A. Empfield, J. Na, E. Blair and L.-S. Fan, *Appl. Energy*, 2016, **165**, 183–201.
21 A. Tong, S. Bayham, M. V. Kathe, L. Zeng, S. Luo and L.-S. Fan, *Appl. Energy*, 2014, **113**, 1836–1845.
22 L. Qin, M. Guo, Z. Cheng, M. Xu, Y. Liu, D. Xu, J. A. Fan and L.-S. Fan, *J. Mater. Chem. A*, 2017, **5**, 20153–20160.
23 D. Li, R. Xu, X. Li, Z. Li, X. Zhu and K. Li, *Energy & Fuels*, 2020, **34**, 5381–5413.
24 M. Fathi, E. Bjorgum, T. Viig and O. Rokstad, *Catal. Today*, 2000, **63**, 489–497.
25 Y. Liu, L. Qin, Z. Cheng, J. Goetze, F. Kong, J. A. Fan and L.-S. Fan, *Nat. Commun.*, 2019, (10), 1–6.
26 K. Otsuka, E. Sunada, T. Ushiyama and I. Yamanaka, *Stud. Surf. Sci. Catal.*, 1997, **107**, 531–536.
27 K. Otsuka, Y. Wang, E. Sunada and I. Yamanaka, *J. Catal.*, 1998, **175**, 152–160.
28 L. F. De Diego, M. Ortiz, J. Adánez, F. García-Labiano, A. Abad and P. Gayán, *Chem. Eng. J.*, 2008, **144**, 289–298.
29 F. He, Y. Wei, H. Li and H. Wang, *Energy Fuels*, 2009, **23**, 2095–2102.
30 G. Azimi, T. Mattisson, H. Leion, M. Rydén and A. Lyngfelt, *Int. J. Greenhouse Gas Control*, 2015, **34**, 12–24.
31 A. Pineau, N. Kanari and I. Gaballah, *Thermochim. Acta*, 2007, 45675–45688.
32 L.-S. Fan, L. Zeng and S. Luo, *AIChE J.*, 2015, **61**, 2–22.
33 L. Qin, M. Guo, Y. Liu, Z. Cheng, J. A. Fan and L.-S. Fan, *Appl. Catal., B*, 2018, **235**, 143–149.
34 L. Qin, Z. Cheng, M. Guo, M. Xu, J. A. Fan and L.-S. Fan, *ACS Energy Lett.*, 2017, **2**, 70.
35 D. Zhao, J. Feng, Q. Huo, N. Melosh, G. H. Fredrickson, B. F. Chmelka and G. D. Stucky, *Science*, 1998, **279**, 548–552.
36 A. Abad, F. García-Labiano, L. F. de Diego, P. Gayán and J. Adánez, *Energy Fuels*, 2007, **21**(4), 1843–1853.
37 www.acsmaterial.com/sba-16.html.
38 S. Luo, L. Zeng, D. Xu, M. Kathe, E. Y. Chung, N. Deshpande, L. Qin, A. Majumder, T.-L. Hsieh, A. Tong, Z. Sun and L.-S. Fan, *Energy Environ. Sci.*, 2014, **7**, 4104.
39 M. Y. Sinev, Z. T. Fattakhova, V. I. Lomonosov and Y. A. Gordienko, *J. Nat. Gas Chem.*, 2009, **18**, 273–287.
40 J. A. Labinger, *Catal. Lett.*, 1988, **1**, 371–376.
41 J. W. M. H. Geerts, Q. Chen, J. M. N. van Kasteren and K. van der Wiele, *Catal. Today*, 1990, **6**, 519–526.
42 V. R. Choudhary and B. S. Uphade, *Catal. Surv. Asia*, 2004, **8**, 15–25.
43 G. E. Keller and M. M. Bhasin, *J. Catal.*, 1982, **73**, 9–19.
44 C. Shi, M. P. Rosynek and J. H. Lunsford, *J. Phys. Chem.*, 1994, **98**, 8371–8376.
45 J. Garcia-Fayos Julio, M. P. Lobera, M. Balaguer and J. M. Serra, *Front. Mater.*, 2018, **5**, 31.
46 Y. S. Su, J. Y. Ying and W. H. Green Jr, *J. Catal.*, 2003, **218**, 321–333.
47 B. L. Farrell, O. I. Valentina and S. Linic, *ACS Catal.*, 2016, **6**, 4340–4346.
48 A. Cruellas, T. Melchiori, F. Gallucci and A. M. van Sint, *Catal. Rev.: Sci. Eng.*, 2017, **59**, 234–294.
49 A. M. Maitra, C. Sacchetta and R. J. Tyler, *Stud. Surf. Sci. Catal.*, 1994, **81**, 261–263.
50 L. Mleczko, U. Pannek, M. Rothaemel and M. Baerns, *Can. J. Chem. Eng.*, 1996, **74**, 279–287.
51 G. S. Lane and E. W. Eduardo, *J. Catal.*, 1988, **113**, 144–163.
52 J. H. Lunsford, *Catal. Today*, 1990, **6**, 235–259.
53 L. Luo, X. Tang, W. Wang, Y. Wang, S. Sun, F. Qi and W. Huang, *Sci. Rep.*, 2013, **3**, 1–6.
54 Z. Cheng, D. S. Baser, S. G. Nadgouda, L. Qin, J. A. Fan and L.-S. Fan, *ACS Energy Lett.*, 2018, **3**, 1730–1736.
55 J. A. Sofranko, J. J. Leonard, C. A. Jones, A. M. Gaffney and H. P. Withers, *Catal. Today*, 1988, **3**, 127–135.
56 A. M. Gaffney, C. A. Jones, J. J. Leonard and J. A. Sofranko, *J. Catal.*, 1988, **114**, 422–432.
57 G. E. Keller and M. M. Bhasin, *J. Catal.*, 1982, **73**, 9–19.
58 C. A. Jones, J. J. Leonard and J. A. Sofranko, *U.S. Pat.*, 4443644444364544436464443647443648444364944449 84, 1984.
59 C. A. Jones, J. J. Leonard and J. A. Sofranko, *Energy Fuels*, 1987, **1**, 12–16.
60 W. P. Schammel, J. Wolfenbarger, M. Ajinkya, J. McCarty, J. M. Cizeron, S. Weinberger and F. R. Zurcher, 2017, *U.S. Pat.*, 9556086.
61 http://siluria.com/Technology/Demonstration_Plant.
62 http://siluria.com/Products/Gemini_-_Natural_Gas_to_Ethylene.
63 X. Zhu, Q. Imtiaz, F. Donat, C. R. Müller and F. Li, *Energy Environ. Sci.*, 2020, **13**, 772–804.
64 C. A. Jones, J. J. Leonard and J. A. Sofranko, *Energy Fuels*, 1987, **1**, 12–16.
65 J. S. Sung, K. Y. Choo, T. H. Kim, A. Greish, L. Glukhov, E. Finashina and L. Kustov, *Appl. Catal., A*, 2010, **380**, 28–32.
66 V. Fleischer, P. Littlewood, S. Parishan and R. Schomäcker, *Chem. Eng. J.*, 2016, **306**, 646–654.

67 V. Fleischer, U. Simon, S. Parishan, M. G. Colmenares, O. Görke, A. Gurlo and K. P. Dinse, *J. Catal.*, 2018, **360**, 102–117.
68 A. A. Greish, L. M. Glukhov, E. D. Finashina, L. M. Kustov, J. S. Sung, K. Y. Choo and T. H. Kim, *Mendeleev Commun.*, 2010, **1**, 28–30.
69 L. M. Ioffe, P. Bosch, T. Viveros, H. Sanchez and Y. G. Borodko, *Mater. Chem. Phys.*, 1997, **51**, 269–275.
70 E. Y. Chung, W. K. Wang, S. G. Nadgouda, D. S. Baser, J. A. Sofranko and L.-S. Fan, *Ind. Eng. Chem. Res.*, 2016, **55**, 12750–12764.
71 J. Wu, S. Li, J. Niu and X. Fang, *Appl. Catal., A*, 1995, **124**, 9–18.
72 K. Takanabe and E. Iglesia, *J. Phys. Chem. C*, 2009, **113**, 10131–10145.
73 S. Arndt, T. Otremba, U. Simon, M. Yildiz, H. Schubert and R. Schomäcker, *Appl. Catal., A*, 2012, **425**, 53–61.
74 Z.-C. Jiang, G. Hua and S.-B. Li, *Stud. Surf. Sci. Catal.*, 1997, **112**, 481–490.
75 D. Kiani, S. Sourav, J. Baltrusaitis and I. E. Wachs, *ACS Catal.*, 2019, **9**, 5912–5928.
76 F. Ali and S. Mansouri, *Arabian J. Chem.*, 2016, **9**, S28–S34.
77 U. Zavyalova, M. Geske, R. Horn, G. Weinberg, W. Frandsen, M. Schuster and R. Schlogl, *ChemCatChem*, 2011, **3**, 949.
78 A. Farsi, A. Moradi, S. Ghader and V. Shadravan, *Chin. J. Chem. Phys.*, 2011, **24**(1), 70–76.
79 M. Yildiz, Y. Aksu, U. Simon, T. Otremba, K. Kailasam, C. Göbel, F. Girgsdies, O. Görke, F. Rosowski, A. Thomas, R. Schomäcker and S. Arndt, *Appl. Catal., A*, 2016, **525**, 168–179.
80 K. Takanabe, A. M. Khan, Y. Tang, L. Nguyen, A. Ziani, B. W. Jacobs, A. M. Elbaz, S. M. Sarathy and F. F. Tao, *Angew. Chem.*, 2017, **129**(35), 10539–10543.
81 S. Mahmoodi, M. R. Ehsani and S. M. Ghoreishi, *J. Ind. Eng. Chem.*, 2010, **16**, 923–928.
82 J. S. Lee and S. T. Oyama, *Catal. Rev.: Sci. Eng.*, 1988, **30**, 249–280.
83 G. J. Hutchings, M. S. Scurrell and J. R. Woodhouse, *Chem. Soc. Rev.*, 1989, **18**, 251–283.
84 J. A. Sofranko and J. C. Jubin, *Symposium on Methane Activation, Conversion, and Utilization. International Congress of Pacific Basin Societies*, Honololu, HI, 1989.
85 http://siluria.com/Technology/Ethylene_to_Liquids.
86 C. A. Jones, J. J. Leonard and J. A. Sofranko, *Energy Fuels*, 1987, **1**, 12–16.
87 H. R. Godini, S. Xiao, S. Jašo, S. Stünkel, D. Salerno, N. X. Son and G. Wozny, *Fuel Process. Technol.*, 2013, **106**, 684–694.
88 V. Spallina, I. C. Velarde, J. A. M. Jimenez, H. R. Godini, F. Gallucci and M. V. S. Annaland, *Energy Convers. Manage.*, 2017, **154**, 244–261.
89 K. M. Sundaram and G. F. Froment, *Chem. Eng. Sci.*, 1977, **32**, 601–608.
90 I. Amghizar, L. A. Vandewalle, K. M. Van Geem and G. B. Marin, *Engineering*, 2017, **3**, 171–178.
91 V. P. Haribal, L. M. Neal and F. Li, *Energy*, 2017, **119**, 1024–1035.
92 L. M. Neal, S. Yusuf, J. A. Sofranko and F. Li, *Energy Technol.*, 2016, **4**, 1200–1208.
93 G. P. Froment, B. O. Van de Steene, P. S. Van Damme, S. Narayanan and A. G. Goossens, *Ind. Eng. Chem. Process Des. Dev.*, 1976, **15**, 495–504.
94 J. V. Moreira, *Steam cracking: kinetics and feed characterisation*, Instituto Superior Tecnico, Lisbon, Portugal, 2015.
95 A. S. Bodke, D. Henning, L. D. Schmidt, S. S. Bharadwaj, J. J. Maj and J. Siddall, *J. Catal.*, 2000, **191**, 62–74.
96 Y. Brik, M. Kacimi, M. Ziyad and F. Bozon-Verduraz, *J. Catal.*, 2001, **202**, 118–128.
97 C. A. Gartner, A. C. van Veen and J. A. Lercher, *ChemCatChem*, 2013, **5**, 3196–3217.
98 F. Cavani, N. Ballarini and A. Cericola, *Catal. Today*, 2007, **127**, 113–131.
99 E. Heracleous and A. A. Lemonidou, *J. Catal.*, 2006, **237**, 162–174.
100 Y. Seif, H. Vasudev, J. Daniel, N. Luke and F. Li, *Appl. Catal., B*, 2019, **257**, 117885.
101 S. Yusuf, L. M. Neal and F. Li, *ACS Catal.*, 2017, **7**, 5163–5173.
102 S. Yusuf, L. Neal, Z. Bao, Z. Wu and F. Li, *ACS Catal.*, 2019, **9**, 3174–3186.
103 Y. Gao, F. Haeri, F. He and F. Li, *ACS Catal.*, 2018, **8**, 1757–1766.
104 Y. Gao, L. M. Neal and F. Li, *ACS Catal.*, 2016, **6**, 7293–7302.
105 S. Chen, L. Zeng, R. Mu, C. Xiong, Z. J. Zhao, C. Zhao, C. Pei, L. Peng, J. Luo, L.-S. Fan and J. Gong, *J. Am. Chem. Soc.*, 2019, **141**, 18653–18657.
106 J. J. Sattler, J. Ruiz-Martinez, E. Santillan-Jimenez and B. M. Weckhuysen, *Chem. Rev.*, 2014, **114**, 10613–10653.
107 D. Sanfilippo and I. Miracca, *Catal. Today*, 2006, **111**, 133–139.
108 I. Miracca and L. Piovesan, *Catal. Today*, 1999, **52**, 259–269.
109 Z. Nawaz and F. Wei, *Ind. Eng. Chem. Res.*, 2009, **48**, 7442–7447.
110 I. Miracca and L. Piovesan, *Catal. Today*, 1999, **52**, 259–269.
111 G. A. Olah and A. Molnar, *Hydrocarbon Chemistry*, 2003, vol. 2, p. 30.
112 N. Rahimi and R. Karimzadeh, *Appl. Catal., A*, 2011, **398**, 1.
113 M. Sarazen and C. Jones, *J. Phys. Chem. C*, 2018, **122**, 28637–28644.
114 D. Mudit, K. Pavlo and M. Giannis, *ACS Catal.*, 2018, **8**, 11570–11578.
115 J. Venegas, W. McDermott and I. Hermans, *Acc. Chem. Res.*, 2018, **51**, 2556.
116 L. Zeng, Z. Cheng, J. A. Fan, L.-S. Fan and J. Gong, *Nat. Rev. Chem.*, 2018, **2**, 349–364.
117 N. Ballarini, A. Battisti, F. Cavani, A. Cericola, C. Cortelli, M. Ferrari, F. Trifirò and P. Arpentinier, *Appl. Catal., A*, 2006, **307**, 148.
118 D. Creaser, B. Andersson, R. R. Hudgins and P. L. Silveston, *Chem. Eng. Sci.*, 1999, **54**, 4437.

119 O. Rubio, J. Herguido and M. Menéndez, *Chem. Eng. Sci.*, 2003, **58**, 461.
120 I. A. Bakare, S. A. Mohamed, S. Al-Ghamdi, S. A. Razzak, M. M. Hossain and H. I. de Lasa, *Chem. Eng. J.*, 2015, **278**, 207.
121 S. Al-Ghamdi, M. Volpe, M. M. Hossain and H. de Lasa, *Appl. Catal., A*, 2013, **450**, 120.
122 A. Qiao, V. N. Kalevaru, J. Radnik, A. Düvel, P. Heitjans, A. S. H. Kumar, P. S. S. Prasad, N. Lingaiah and A. Martin, *Ind. Eng. Chem. Res.*, 2014, **53**, 18711.
123 B. M. Weckhuysen and D. E. Keller, *Catal. Today*, 2003, **78**, 25.
124 A. H. Elbadawi, M. S. Ba-Shammakh, S. Al-Ghamdi, S. A. Razzak, M. M. Hossain and H. I. de Lasa, *Chem. Eng. Sci.*, 2016, **145**, 59.
125 N. Ballarini, F. Cavani, M. Ferrari, R. Catani and U. Cornaro, *J. Catal.*, 2003, **213**, 95.
126 H. Yang, S. Yuanjun and L. Siris, *ACS Catal.*, 2019, **9**, 10464–10468.
127 A. Ayandiran, I. Bakare, H. Binous, S. Al-Ghamdi, S. Razzak and M. Hossain, Oxidative dehydrogenation of propane to propylene over VOx/CaO–γ-Al2O3 using lattice oxygen, *Catal. Sci. Technol.*, 2016, **6**, 5154–5167.
128 A. S. Russell and J. J. Stokes, *Ind. Eng. Chem.*, 1946, **38**, 1071.
129 S. Xie, K. Chen, A. T. Bell and E. J. Iglesia, *J. Phys. Chem. B*, 2000, **104**, 10059.
130 R. López Cordero, F. J. Gil Llambias and A. López Agudo, *Appl. Catal.*, 1991, **74**, 125.
131 P. C. H. Mitchell and S. A. Wass, *Appl. Catal., A*, 2002, **225**, 153.
132 N. S. Gnep, J. Y. Doyemet, A. M. Seco, F. R. Ribeiro and M. Guisnet, *Appl. Catal.*, 1988, **43**, 155.
133 N. S. Nesterenko, O. A. Ponomoreva, V. V. Yuschenko, I. I. Ivanova, F. Testa, F. Di Renzo and F. Fajula, *Appl. Catal., A*, 2003, **254**, 261–272.
134 B. Xu, B. Zheng, W. Hua, Y. Yue and Z. Gao, *J. Catal.*, 2006, **239**, 470.
135 B. Xu, T. Li, B. Zheng, W. Hua, Y. Yue and Z. Gao, *Catal. Lett.*, 2007, **119**, 283.
136 C.-T. Shao, W.-Z. Lang, X. Yan and Y.-J. Guo, *RSC Adv.*, 2017, **7**, 4710.
137 S. A. Al-Ghamdi and H. I. de Lasa, *Fuel*, 2014, **128**, 120–140.
138 M. Volpe, G. Tonetto and H. de Lasa, *Appl. Catal., A*, 2004, **272**, 69.
139 S. D. Jackson and S. J. Rugmini, *J. Catal.*, 2007, **251**, 59.
140 M. E. Harlin, V. M. Niemi, A. O. I. Krause and B. M. Weckhuysen, *J. Catal.*, 2001, **203**, 242.
141 T. V. M. Rao and G. Deo, *AIChE J.*, 2007, **53**, 2432–2442.
142 M. E. Harlin, L. B. Backman, A. O. I. Krause and O. J. T. Jylhä, *J. Catal.*, 1999, **183**, 300.
143 M. E. Harlin, A. O. I. Krause, B. Heinrich, C. Pham-huu and M. J. Ledoux, *Appl. Catal., A*, 1999, **185**, 311.
144 M. Saito, S. Watanabe, I. Takahara, M. Inaba and K. Murata, *Catal. Lett.*, 2003, **89**, 213.
145 J. H. Yun and R. F. Lobo, *J. Catal.*, 2014, **312**, 263.
146 H. Shimada, T. Akazawa, N. Ikenaga and T. Suzuki, *Appl. Catal., A*, 1998, **168**, 243.
147 http://pet-oil.blogspot.nl/2012/10/uop-oleflex-process-for-light-olefin.html.
148 http://www.cbi.com/images/uploads/tech_sheets/CatofinDehyrogenation-12.pdf.
149 S. Chen, L. Zeng, R. Mu, C. Xiong, Z. J. Zhao, C. Zhao, C. Pei, L. Peng, J. Luo, L.-S. Fan and J. Gong, *J. Am. Chem. Soc.*, 2019, **141**, 18653–18657.